

Atomically self-healing of structural defects in monolayer WSe_2

Kangshu Li(李康舒), Junxian Li(李俊贤), Xiaocang Han(韩小藏), Wu Zhou(周武), and Xiaoxu Zhao(赵晓续)

Citation: Chin. Phys. B, 2024, 33 (**9**): 096804. DOI: 10.1088/1674-1056/ad641f
Journal homepage: http://cpb.iphy.ac.cn; http://iopscience.iop.org/cpb

What follows is a list of articles you may be interested in

Electronic structure engineering of transition metal dichalcogenides for boosting hydrogen energy conversion electrocatalysts

Bing Hao(郝兵), Jingjing Guo(郭晶晶), Peizhi Liu(刘培植), and Junjie Guo(郭俊杰)
Chin. Phys. B, 2024, 33 (**9**): 096802. DOI: 10.1088/1674-1056/ad625b

Surface evolution of thermoelectric material KCu_4Se_3 explored by scanning tunneling microscopy

Yumin Xia(夏玉敏), Ni Ma(马妮), Desheng Cai(蔡德胜), Yuzhou Liu(刘宇舟), Yitong Gu(谷易通), Gan Yu(于淦), Siyu Huo(霍思宇), Wenhui Pang(庞文慧), Chong Xiao(肖翀), and Shengyong Qin(秦胜勇)
Chin. Phys. B, 2024, 33 (**8**): 086804. DOI: 10.1088/1674-1056/ad50c4

Controlled fabrication of freestanding monolayer SiC by electron irradiation

Yunli Da(笪蕴力), Ruichun Luo(罗瑞春), Bao Lei(雷宝), Wei Ji(季威), and Wu Zhou(周武)
Chin. Phys. B, 2024, 33 (**8**): 086802. DOI: 10.1088/1674-1056/ad6132

Optimal parameter space for stabilizing the ferroelectric phase of $Hf_{0.5}Zr_{0.5}O_2$ thin films under strain and electric fields

Lvjin Wang(王侣锦), Cong Wang(王聪), Linwei Zhou(周霖蔚), Xieyu Zhou(周谐宇), Yuhao Pan(潘宇浩), Xing Wu(吴幸), and Wei Ji(季威)
Chin. Phys. B, 2024, 33 (**7**): 076803. DOI: 10.1088/1674-1056/ad498b

Growth and characterization of Bi(110)/$CrTe_2$ heterostructures: Exploring interplay between magnetism and topology

Zhenyu Yuan(袁震宇), Fazhi Yang(杨发枝), Baiqing Lv(吕佰晴), Yaobo Huang(黄耀波), Tian Qian(钱天), Jinpeng Xu(徐金朋), and Hong Ding(丁洪)
Chin. Phys. B, 2024, 33 (**2**): 026802. DOI: 10.1088/1674-1056/ad082a

---

SPECIAL TOPIC — Stephen J. Pennycook: A research life in atomic-resolution STEM and EELS

Atomically self-healing of structural defects in monolayer WSe_2

Kangshu Li(李康舒)[1], Junxian Li(李俊贤)[1], Xiaocang Han(韩小藏)[1], Wu Zhou(周武)[2], and Xiaoxu Zhao(赵晓续)[1,3,†]

[1] *School of Materials Science and Engineering, Peking University, Beijing* 100871, *China*
[2] *School of Physical Sciences, University of Chinese Academy of Sciences, Beijing* 100049, *China*
[3] *AI for Science Institute, Beijing* 100084, *China*

(Received 1 May 2024; revised manuscript received 12 July 2024; accepted manuscript online 17 July 2024)

Minimizing disorder and defects is crucial for realizing the full potential of two-dimensional transition metal dichalcogenides (TMDs) materials and improving device performance to desired properties. However, the methods in defect control currently face challenges with overly large operational areas and a lack of precision in targeting specific defects. Therefore, we propose a new method for the precise and universal defect healing of TMD materials, integrating real-time imaging with scanning transmission electron microscopy (STEM). This method employs electron beam irradiation to stimulate the diffusion migration of surface-adsorbed adatoms on TMD materials grown by low-temperature molecular beam epitaxy (MBE), and heal defects within the diffusion range. This approach covers defect repairs ranging from zero-dimensional vacancy defects to two-dimensional grain orientation alignment, demonstrating its universality in terms of the types of samples and defects. These findings offer insights into the use of atomic-level focused electron beams at appropriate voltages in STEM for defect healing, providing valuable experience for achieving atomic-level precise fabrication of TMD materials.

Keywords: scanning transmission electron microscopy (STEM), atom manipulation, nanoscale materials and structures: fabrication and characterization, new materials: theory, design, fabrication

PACS: 68.37.Ma, 81.16.Ta, 81.07.–b, 81.05.Zx **DOI:** 10.1088/1674-1056/ad641f

1. Introduction

Semiconducting transition metal dichalcogenides (TMDs) such as MoS_2, $MoSe_2$, WS_2, WSe_2, and $MoTe_2$ are promising two-dimensional materials. Their two-dimensional structure allows for the modulation of bandgaps through adjustments in thickness, strain, and stacking sequences.[1–3] Additionally, the weak van der Waals (vdW) forces between layers in these materials facilitate the formation of flexible, stacked vdW heterostructures without the constraints of lattice matching. These characteristics collectively enhance the capability for precise atomic-scale engineering of band structures, expanding the possibilities for creating innovative materials tailored for electronic applications.[4] The diminished screening and enhanced electron–hole interactions in two-dimensional TMDs, relative to traditional semiconductors, endow these materials with robust spectral properties and suitability for electronic device applications.[4,5]

However, chalcogen atomic defects exist inherently in 2D TMDs and may be introduced intrinsically or extrinsically during the synthesis or through post-growth treatment.[6,7] Achieving large-scale growth of TMD films with a minimal defect density remains an unrealized goal, representing a bottleneck for the integration of 2D electronics into industrial applications. As a key objective of defect engineering, deliberately inducing atomic defects[8,9] in a controlled manner can effectively alter the physical and chemical properties of TMDs. However, in numerous instances, defects are detrimental as they can diminish the properties and device performances of TMDs.[10] Notably, the widespread chalcogen vacancies act as major traps, electron dopants, and/or scattering centers of carriers, resulting in deteriorated electronic or optoelectronic properties.[11–14] These scattering centers, which limit electron mobility, have been both theoretically described[12,15–21] and experimentally characterized,[19–21] making them the most limiting factors for the reduced electron mobility,[9] thereby limiting the scope of application. WSe_2 is a p-type semiconductor that theoretically possesses extraordinary electronic properties. However, its application across a broader spectrum is restricted due to material quality, particularly due to point defects, line defects, and so on.[22] Therefore, healing of chalcogen atomic defects provides a powerful tool for enhancing the properties and device performances of 2D TMDs, while avoiding adverse effects.

In addition to the controlled creation of defects and their quantification in 2D materials, the healing of defects is another important topic of defects engineering. Common methods for healing defects in TMDs can generally be categorized into dry gas-phase treatment[23–27] and wet liquid-phase process.[28,29] Due to the fragility of monolayer TMDCs, dry gas-phase treatment is more widely selected and applied. However, the works reported so far generally target macroscopic areas exposed to gas or liquid phases for defect healing, making it difficult to experimentally achieve a precise selection of the defect sites to be repaired.[24,30,31] The capacity to manipulate

†Corresponding author. E-mail: xiaoxuzhao@pku.edu.cn

© 2024 Chinese Physical Society and IOP Publishing Ltd

and engineer atomic structures and dynamics brings us ever closer to achieving one of the ultimate goals in nanoscience and nanotechnology: precise control over matter at the atomic level and harnessing the unique properties that emerge at the nanoscale. With the rapid advancements in STEM, atomically focused e-beam in STEM is not only useful for imaging and analysis,[32] but also serves as a powerful tool for atomic-level defect manipulation.[33–35]

In this paper, we demonstrate a universally applicable defect healing method that uses electron beam irradiation to induce surface-adsorbed selenium adatoms to repair multi-type defects in monolayer WSe_2 grown by molecular beam epitaxy (MBE). In ADF-STEM (annular dark-field) irradiation real-time imaging experiments, various types of repair phenomena were observed, including repairing single defects, multiple defects (holes), grain boundary repairs, and grain orientation alignment. The scope of defect repair extends universally from 0D to 2D. Our results make a step forward for the realization of high-precision atomic assembly in TMDs and open a new avenue to achieve high-quality TMD materials through defect repair. The straightforward prerequisites make this method promising for widespread adoption across all TMD materials.

2. Results and discussion

2.1. Defect healing in monolayer WSe_2 under electron beam irradiation

We first demonstrate the process of healing single vacancy defects via electron beam irradiation-induced surface adsorbed Se atom migration, using monolayer 1H-WSe_2 as an example, as illustrated in Figs. 1(a) and 1(b). Figure 1(a) shows that monolayer WSe_2, induced by electron irradiation to adsorb surface atoms, is synthesized on a SiO_2 substrate at a low temperature of 200 °C via MBE, and is then transferred onto an electron microscopy copper microgrid coated with conductive carbon film. Reported computational results[36] indicate that the nucleation and growth mechanisms of vdW two-dimensional materials via MBE differ from the traditional growth modes of three-dimensional materials, following a three-step mechanism of adsorption–diffusion–attachment. It is shown that the adatom stage plays an important role in the nucleation. Therefore, compared to chemical vapor deposition (CVD),[37] monolayer WSe_2 grown under the relatively low temperature of 200 °C and ultra-high vacuum conditions (3×10^{-10} mbar) inevitably possesses surface-adsorbed adatoms.[38]

The surface-adsorbed selenium atoms preserved by low-temperature MBE growth and the conductive carbon film on the microgrid are prerequisites for defect healing via electron beam irradiation, as discussed later. Theoretically, electron beam irradiation results in energy transfer that can lead to two opposing effects: an increase in defect concentration due to irradiation (ionization and/or knock-on) damage, and defect healing facilitated by the migration of surface-adsorbed atoms. The semiconducting monolayer WSe_2, transferred onto the microgrid, is subjected to electron beam irradiation. Since the sample is in direct contact with the conducting carbon film on the microgrid, the improved conductivity could quickly dissipate the impinging high-energy electrons, this setup eliminates the potential for ionization damage (radiolysis) that could be caused by the stimulated movement of atoms.[39]

According to a reported work,[19] the displacement threshold (T_d) for selenium atoms in monolayer WSe_2 has been calculated using density functional theory (DFT) to be around 6.4 eV.[40] Based on the McKinley–Feshbach formalism,[41] the electron threshold energy can be estimated by calculating T_d. Similar to monolayer $MoSe_2$, the formation of selenium vacancies in monolayer WSe_2 through the knock-on damage mechanism requires an electron acceleration voltage of at least 200 kV,[19,40] which is significantly lower than the 80 kV used in STEM imaging for this experiment. Additionally, the ultra-high vacuum and the temperature of 200 °C during sample synthesis essentially free the sample surface from the presence of polymer residues that could cause chemical etching effects. This is also evidenced by the clear STEM experimental images, which show no areas with uneven contrast akin to a foggy dispersion.

Given that the sample characteristics and environment do not facilitate radiation damage, the energy of the electron beam will be transferred to the surface-adsorbed Se adatoms via elastic collisions, initiating other atomic motions.[42–45] When bombarded with a 60 kV electron beam, the energy transferred to the Se atoms can reach 1.8 eV,[40] sufficient to overcome the energy barrier for free diffusion on monolayer WSe_2 (0.23 eV).[46] Therefore, kinetically, surface-adsorbed Se adatoms can undergo diffusion migration across the sample surface, and thermodynamically, the incorporation of Se atoms into vacancy sites reduces the total energy of the system. Thus, using a 100 kV electron beam to facilitate the surface diffusion migration of Se atoms for defect repair is feasible. By employing STEM imaging technology with low electron acceleration voltage, not only is the monolayer WSe_2 robust under electron beam irradiation, but it also provides sufficient energy for the diffusion and migration of adsorbed Se adatoms during real-time imaging observation.

2.2. Tracking the migration sites of Se adatoms in healing single vacancies

To unveil the atomic-scale healing of Se vacancies in monolayer WSe_2 through the migration of Se adatoms, we analyzed the atomic structure and chemical composition of both pristine and repaired monolayer WSe_2 using ADF-STEM. The intensity observed in the ADF-STEM images reveals a Z^n-contrast relationship (Z: atomic number, $n = 1.6$–2),[47] stem-

ming from its incoherent nature. This allows for direct quantification of the number of individual atoms in each atomic column in samples of known thickness. Leveraging this imaging feature, atom-by-atom chemical identification and configurative analysis of defects and local concentrations have been achieved through quantitative analysis of the monolayer WSe_2 via ADF-STEM. To observe the actual single defect healing mechanism *in situ*, sequential ADF-STEM imaging was employed. Figures 1(c)–1(h) show the healing process for two selenium vacancy sites under e-beam irradiation (44 s, 8.8×10^6 $e^- \cdot \mathrm{nm}^{-2}$). The top row of images displays five selected ADF-STEM images of the monolayer WSe_2 sample, presenting the typical hexagonal lattice of the 1H phase of monolayer WSe_2. Due to the Z contrast nature of ADF-STEM imaging, W atoms ($Z = 74$) appear brighter than Se_2 ($Z = 34$) atom columns.[48] Vacancies at single Se atoms and double Se atoms appear darker than the columns of W and Se_2 atoms.

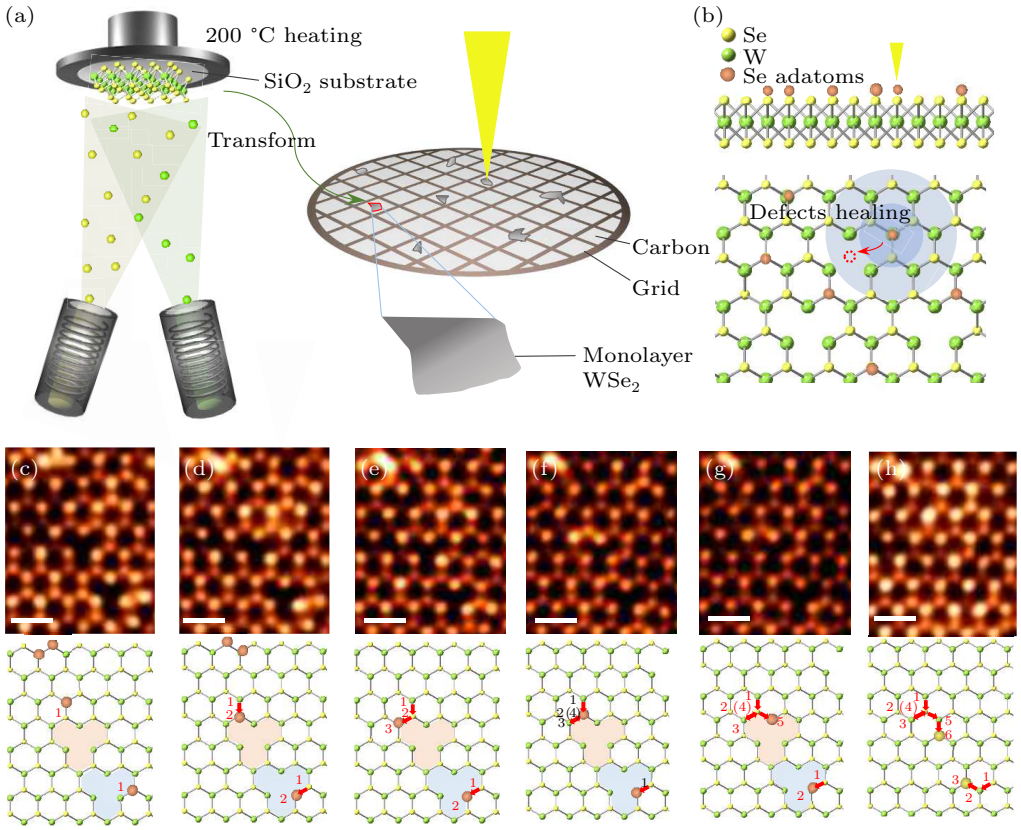


Fig. 1. The experiment setup and a complete process of defects healing in monolayer WSe_2. (a) Schematic illustration showing the formation of monolayer WSe_2 with adatoms at a low temperature of 200 °C through MBE, and transformation from substrate to a Cu skeleton micro-grid supported by amorphous carbon films. In the environment of a spherical aberration-corrected electron microscope, it undergoes irradiation by an electron beam probe utilized for STEM imaging. (b) Side and top-view atomic models of monolayer WSe_2 subjected to e-beam irradiation, where yellow spheres represent selenium atoms within the lattice structure, green spheres denote tungsten atoms, and orange spheres are indicative of surface-adsorbed selenium adatoms. (c)–(h) Sequential ADF-STEM images displaying defects annihilations upon e-beam irradiation for (c) 0 s, (d) 13 s, (e) 21 s, (f) 28 s, (g) 41 s, and (h) 44 s respectively, in monolayer WSe_2. Corresponding atomic models are depicted on the lower panels, with the pathways of two Se adatoms highlighted by arrows. The diffusion process of the top selenium contains six steps, whereas only three steps are associated with the bottom selenium atom. Scale bars: 0.5 nm.

Based on the variations in brightness at specific sites in the ADF-STEM images, it is possible to atomically track the Se atoms healing the Se vacancies originating from surface-adsorbed Se adatoms. The surface-adsorbed Se adatom used to heal the Se vacancy above (marked with an orange polygon) undergoes six diffusion steps and five adsorption sites from their initial state, covering a maximum linear diffusion distance of 4.8 Å, ultimately completing the vacancy repair, filling the double Se vacancies to form a single Se vacancy. Meanwhile, the double Se vacancy defects below (marked with a blue polygon) are also repaired by surface-adsorbed selenium atoms through a three-step migration, reducing them to single Se vacancies. Cases similar to those shown in Figs. 1(c)–1(h), where surface-adsorbed Se adatoms diffuse to repair single vacancy defects, are very common in sequential STEM imaging, with more examples listed and analyzed in the supplementary information (supplementary Fig. 1).

2.3. Extended vacancies or holes defects healing

In addition to the most common single vacancy defects, clusters of vacancies forming extended vacancies or holes are also common defects affecting the quality of monolayer WSe_2. The presence of holes, unlike single vacancy defects, causes displacements and distortions in the surrounding in-plane

structure, no longer presenting a standard honeycomb structure, thus lacking standard vacancy sites for healing. Surface-adsorbed Se adatoms repair by first filling the vacancies outside the hole, initially correcting the positional distortions in the hole area to present clear vacancy sites, and then proceeding to fill and repair these vacancies. Figure 2 shows the atomic migration trajectories for indirectly repairing holes by using electron beam irradiation (46 s, 9.2×10^6 $e^- \cdot \mathrm{nm}^{-2}$) to induce the diffusion migration of surface-adsorbed Se adatoms to repair the vacancies around the holes.

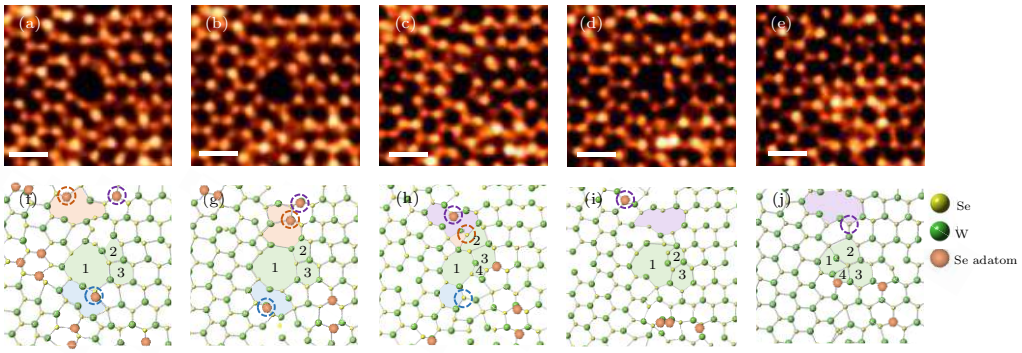


Fig. 2. *In situ* sequential ADF-STEM images depicting the step-by-step healing of extended vacancies or holes in monolayer WSe_2. (a)–(e) Sequential ADF-STEM images of the same region after e-beam irradiation for 0 s, 5 s, 28 s, 36 s, and 46 s, respectively. Adsorbed Se adatoms fill in at lattice sites around the hole, gradually reducing the size of holes to approximately 0.5 nm in diameter. (f)–(j) Corresponding atomic models of (a)–(e). Dashed circles trace the diffusion migration paths of three surface-adsorbed Se atoms around the hole, which repair the in-plane vacancies outside the hole, altering the distribution of atomic structures around the hole and thereby indirectly completing the repair of the hole. The same Se atom is marked with a dashed circle of the same color, and tracked until it fills the in-plane vacancy. Scale bars: 0.5 nm.

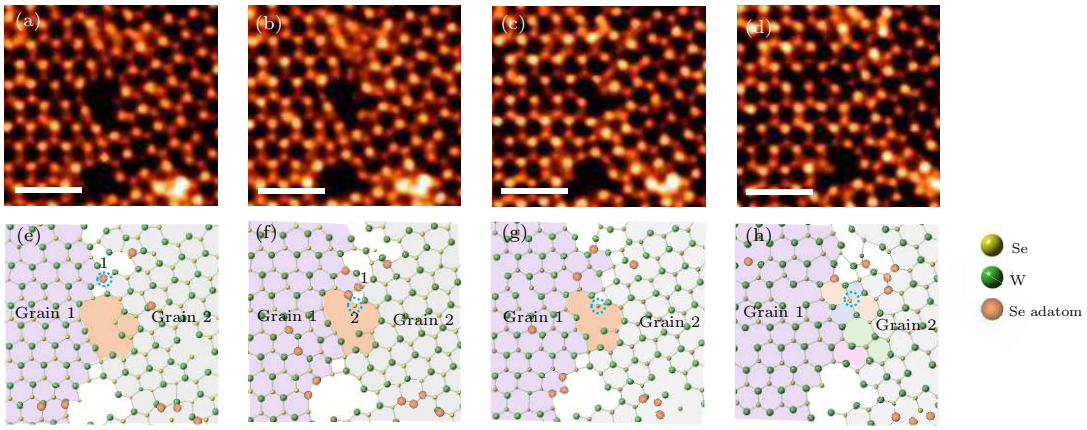


Fig. 3. *In situ* sequential ADF-STEM images depicting the step-by-step healing of extended vacancies or holes at the grain boundary. (a)–(d) Sequential ADF-STEM images of the same region after e-beam irradiation for 0 s, 24 s, 48 s, and 75 s, respectively. (e)–(f) Corresponding atomic model structures of experimental images (a)–(d). The two adjacent grains are marked in grey and purple, respectively, with an inter-grain orientation angle of 10°. Surface-adsorbed Se adatoms complete diffusion migration from site 1 to site 2 and the structural collapse. Centered on the Se atoms repairing the hole, the grid near the grain boundary is repaired, forming 4|5 dislocation cores (marked with a blue polygon), 6|7 dislocation cores (marked with a green polygon), and 6|8 dislocation cores (marked with a pink polygon). Scale bars: 1 nm.

Surface-adsorbed Se adatoms, marked by orange dashed circles, diffuse from an irregular 12-membered ring to a shared Se atom in a 5|7 ring, thereby filling in-plane holes and repairing the 5|6 ring in the area marked by the green polygon 2 and 3 to form nearly hexagonal dual six-membered rings. Meanwhile, surface-adsorbed Se adatom, marked by the blue dashed line, migrates between two W atom sites opposite each other in a decagonal ring and subsequently fills the vacancy within the ring, repairing the decagonal ring into a distorted honeycomb structure. Similarly, surface-adsorbed Se adatoms marked with purple dashed circles aid in correcting structural distortions by filling vacancies, converting a four-membered ring on green polygon 2 into a six-membered ring. As these three surface-adsorbed Se adatoms migrate and repair, the original hole has been repaired into a dislocation-double Se vacancy complex (Se 4|6) (marked by the green polygon 2 and 4), and the uneven strain mapping caused by structural distortions around the hole due to its presence is simultaneously reduced.

In addition to repairing holes within the grains, the diffusion migration of surface-adsorbed Se adatoms can also repair holes at grain boundaries. The interaction between the repaired vacancies and the dislocation cores determines the configuration of the grain boundaries, thereby altering local properties such as the band gap. In the CVD and MBE growth of 2D WSe_2, the resulting WSe_2 is typically polycrystalline, con-

sisting of a honeycomb network of grains with varying crystal orientations, separated by grain boundaries. These grain boundaries are intrinsic 1D topological defects, which in turn are composed of 0D topological defects known as dislocations. However, since the Se–Se and W–W homo-bonds are energetically less favorable than the Se–W hetero-bonds, these dislocations are able to react with Se vacancies or Se interstitials to form dislocation–vacancy or dislocation–interstitial complexes.

Figure 3 illustrates the evolutionary process under e-beam (75 s, 1.5×10^7 $e^- \cdot \mathrm{nm}^{-2}$) where holes at the grain boundary are repaired by the diffusion migration of surface-adsorbed Se atoms into Se 4|5 dislocation cores. At the grain boundary, where the adjacent grain orientation angle is 11°, there is a hole marked by an orange polygon. As surface-adsorbed Se adatom, marked by a blue dashed circle, enters the hole and bonds with the in-plane W atoms of monolayer WSe_2, the initial hole acts as a bonding center, connecting two opposing hexagonal rings as well as opposing four-membered and five-membered rings (Se 4|5, marked by a blue polygon). Besides, the residual vacancy defects interact with the surrounding atoms to form structures such as heptagonal and octagonal rings sharing some atoms, thereby constructing 6|7 dislocation cores (marked by a green polygon) and 6|8 dislocation cores (marked by a pink polygon).

2.4. Grain orientation alignment

Synthesizing high-quality single-crystalline TMD materials from single-crystal nuclei remains an unresolved challenge. This paper proposes that the diffusion migration of surface-adsorbed Se adatoms under electron beam irradiation, by repairing vacancy defects at grain boundaries, can reduce the orientation differences between adjacent grains. Similar to repairing hole defects, surface-adsorbed Se adatoms do not directly affect grain orientation, but can alter the stress field distribution near grain boundaries by diffusing and migrating to fill vacancy defects, indirectly changing the orientation angle between grains.

Figure 4 illustrates the 72 s (1.4×10^7 $e^- \cdot \mathrm{nm}^{-2}$) process of surface-adsorbed Se adatoms filling vacancy defects and the real-time changes in grain orientation and strain distribution. Using the zigzag direction of two grains as a reference, the initial grain orientation difference is 12.9°. As the surface-adsorbed Se adatoms, marked by dashed circles, complete their diffusion migration and fall into vacancies, the diameter of the holes shrinks from about 0.5 nm to approximately 0.2 nm. Defects at the grain boundary are significantly repaired, and the angle reduces to 6.0°. As more surface-adsorbed Se adatoms repair the holes at grain boundary into single Mo polar dislocations (Mo 6|8, marked by orange polygon), the orientation difference between the two grains ultimately narrows to 6.0°.

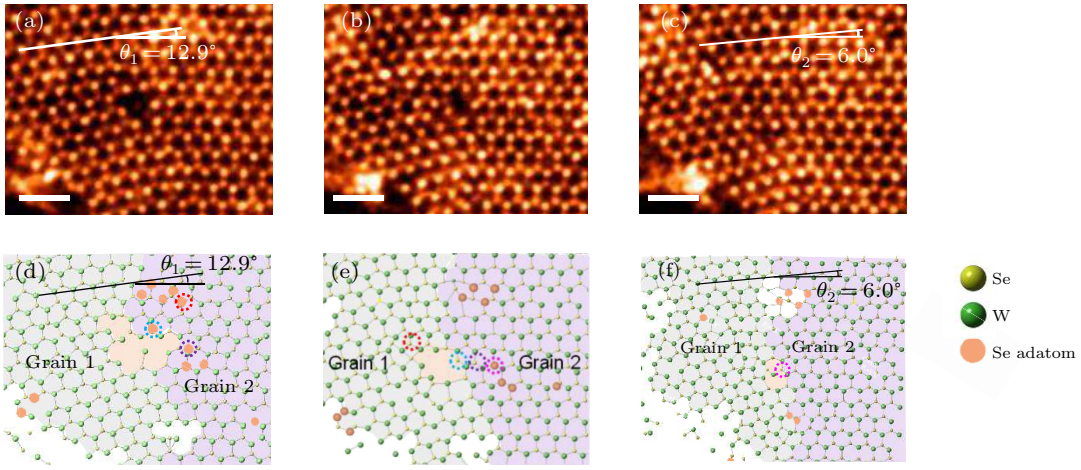


Fig. 4. *In situ* sequential ADF-STEM images depicting the step-by-step grain orientation alignment. (a)–(c) Sequential ADF-STEM images of the same region after e-beam irradiation for 0 s, 27 s and 72 s, respectively. (d)–(f) Corresponding atomic models of (a)–(c). There is a clear grain orientation difference between the upper left grain (marked by grey) and the main body grain on the right (marked by purple). The surface-adsorbed Se adatoms, by diffusing and migrating across the surface of monolayer WSe_2 and repairing vacancies at the grain boundaries, alter the stress field distribution around the grain boundaries, reducing the orientation difference between the grains from 12.9° to 6.0°. Scale bars: 1 nm.

3. Methods

3.1. MBE synthesis

WSe_2 film was grown using an MBE chamber with a base pressure $\sim 6 \times 10^{-10}$ Torr. Before growth, the substrate was degassed in an ultrahigh vacuum chamber for 1 h and annealed at 600 °C for 5 min. For all the experiments, the temperature of the Se crucible cell was maintained at about 180 °C with the cracker at 220 °C. The flux ratio of W/Se was ∼ 1:20. The chamber pressure during growth was $\sim 1 \times 10^{-8}$ Torr.

3.2. STEM characterization

ADF-STEM imaging was performed on an aberration-corrected Nion UltraSTEM100 and Nion U-HERMES200,

equipped with a cold field emission gun. The accelerating voltage was 100 kV for UltraSTEM100 and 60 kV for Nion U-HERMES200, below the knock-on damage threshold of monolayer WSe_2. The convergence semiangle of the probe was around 35 mrad. The collection angle for ADF was between 80 mrad and 200 mrad. The beam current was $\sim$ 15 pA, and the per-pixel dwell time was 4 μs, while the beam intensity was adjusted to realize the continuous change of irradiation doses. The temperature of the electron microscope chamber is stabilized at 22 °C year-round. The column vacuum was $\sim$ 350 pTorr. The ADF-STEM images were filtered by Gaussian filters, and the positions of atomic columns were located by finding the local maxima of the filtered series.

4. Conclusion

In conclusion, our work introduces a novel method for the TMD defects healing via electron beam-induced diffusion migration of surface-adsorbed atoms. The prerequisites for the success of this method include the use of MBE for low-temperature growth to introduce adsorbed atoms, direct contact between the sample and conductive carbon film, and an electron acceleration voltage that is sufficient to overcome migration barriers but remains below the threshold for knock-on damage. The types of defects that can be repaired with this approach are diverse, including vacancies, holes, grain boundaries, and even grain orientation alignment. This method not only optimizes electron mobility and carrier concentration but also furnishes a more stable and reliable substrate for high-performance electronic devices incorporating WSe_2. Monolayer WSe_2 is robust to electron beam irradiation under 100 kV acceleration voltage during STEM imaging, resembling to most TMD materials that can withstand low acceleration voltages with minimal irradiation damage. Therefore, this method has a promising universal application prospect in TMD materials.

Acknowledgments

X.Z. thanks the Beijing Natural Science Foundation (Grant Nos. JQ24010 and Z220020), the Fundamental Research Funds for the Central Universities, and the National Natural Science Foundation of China (Grant No. 52273279). Project supported by the Electron Microscopy Laboratory of Peking University, China for the use of Nion U-HERMES200 scanning transmission electron microscopy. We thank Materials Processing and Analysis Center, Peking University, for assistance with TEM characterization. The electron microscopy work was through a user project at Center of Oak Ridge National Laboratory (ORNL) for Nanophase Materials Sciences (CNMS), which is a DOE Office of Science User Facility.

References

[1] Zhao W, Ghorannevis Z, Chu L, Toh M, Kloc C, Tan P H and Eda G 2013 *ACS Nano* **7** 791
[2] Mak K F, Lee C, Hone J, Shan J and Heinz T F 2010 *Phys. Rev. Lett.* **105** 136805
[3] Ghorbani-Asl M, Borini S, Kuc A and Heine T 2013 *Phys. Rev. B* **87** 235434
[4] Sarkar D, Xie X, Liu W, Cao W, Kang J, Gong Y, Kraemer S, Ajayan P M and Banerjee K 2015 *Nature* **526** 91
[5] Kis A 2012 *Nat. Nanotechnol.* **7** 683
[6] Liang Q, Zhang Q, Zhao X, Liu M and Wee A T S 2021 *ACS Nano* **15** 2165
[7] Mitterreiter E, Schuler B, Micevic A, Hernangómez-Pérez D, Barthelmi K, Cochrane K A, Kiemle J, Sigger F, Klein J, Wong E, Barnard E S, Watanabe K, Taniguchi T, Lorke M, Jahnke F, Finley J J, Schwartzberg A M, Qiu D Y, Refaely-Abramson S, Holleitner A W, Weber-Bargioni A and Kastl C 2021 *Nat. Commun.* **12** 3822
[8] Anon 2012 *Nat. Nanotechnol.* **7** 683
[9] Ippolito S and Samorì P 2022 *Small Sci.* **2** 2100122
[10] Min J, Kim J H and Kang J 2024 *ACS Appl. Nano Mater.*
[11] Yuan L and Huang L 2015 *Nanoscale* **7** 7402
[12] Wang H, Zhang C and Rana F 2015 *Nano Lett.* **15** 339
[13] Hong J, Hu Z, Probert M, Li K, Lv D, Yang X, Gu L, Mao N, Feng Q, Xie L, Zhang J, Wu D, Zhang Z, Jin C, Ji W, Zhang X, Yuan J and Zhang Z 2015 *Nat. Commun.* **6** 6293
[14] Zhu W, Low T, Lee Y H, Wang H, Farmer D B, Kong J, Xia F and Avouris P 2014 *Nat. Commun.* **5** 3087
[15] Caulfield J C and Fisher A J 1997 *J. Phys. Condens. Matter* **9** 3671
[16] Fuhr J D, Saúl A and Sofo J O 2004 *Phys. Rev. Lett.* **92** 26802
[17] Yong K S, Otalvaro D M, Duchemin I, Saeys M and Joachim C 2008 *Phys. Rev. B* **77** 205429
[18] Zhou W, Zou X, Najmaei S, Liu Z, Shi Y, Kong J, Lou J, Ajayan P M, Yakobson B I and Idrobo J C 2013 *Nano Lett.* **13** 2615
[19] Komsa H P, Kotakoski J, Kurasch S, Lehtinen O, Kaiser U and Krasheninnikov A V 2012 *Phys. Rev. Lett.* **109** 35503
[20] Tiwari R K, Yang J, Saeys M and Joachim C 2008 *Surf. Sci.* **602** 2628
[21] Avsar A, Tan J Y, Taychatanapat T, Balakrishnan J, Koon G K W, Yeo Y, Lahiri J, Carvalho A, Rodin A S, O'Farrell E C T, Eda G, Castro Neto A H and Özyilmaz B 2014 *Nat. Commun.* **5** 4875
[22] Zheng Y J, Chen Y, Huang Y L, Gogoi P K, Li M Y, Li L J, Trevisanutto P E, Wang Q, Pennycook S J, Wee A T S and Quek S Y 2019 *ACS Nano* **13** 6050
[23] Pető J, Ollár T, Vancsó P, Popov Z I, Magda G Z, Dobrik G, Hwang C, Sorokin P B and Tapasztó L 2018 *Nat. Chem.* **10** 1246
[24] Lu J, Carvalho A, Chan X K, Liu H, Liu B, Tok E S, Loh K P, Castro Neto A H and Sow C H 2015 *Nano Lett.* **15** 3524
[25] Ma D, Wang Q, Li T, He C, Ma B, Tang Y, Lu Z and Yang Z 2016 *J. Mater. Chem. C* **4** 7093
[26] Mahjouri-Samani M, Liang L, Oyedele A, Kim Y S, Tian M, Cross N, Wang K, Lin M W, Boulesbaa A, Rouleau C M, Puretzky A A, Xiao K, Yoon M, Eres G, Duscher G, Sumpter B G and Geohegan D B 2016 *Nano Lett.* **16** 5213
[27] Fujisawa K, Carvalho B R, Zhang T, Perea-López N, Lin Z, Carozo V, Ramos S L L M, Kahn E, Bolotsky A, Liu H, Elías A L and Terrones M 2021 *ACS Nano* **15** 9658
[28] Zhang X, Liao Q, Liu S, Kang Z, Zhang Z, Du J, Li F, Zhang S, Xiao J and Liu B 2017 *Nat. Commun.* **8** 15881
[29] Roy S, Choi W, Jeon S, Kim D H, Kim H, Yun S J, Lee Y, Lee J, Kim Y-M and Kim J 2018 *Nano Lett.* **18** 4523
[30] Zhao X, Ji Y, Chen J, Fu W, Dan J, Liu Y, Pennycook S J, Zhou W and Loh K P 2019 *Adv. Mater.* **31** 1900237
[31] Hong J, Wang Y, Wang A, Lv D, Jin C, Xu Z, Probert M I J, Yuan J and Zhang Z 2017 *Nanoscale* **9** 10312
[32] Krivanek O L, Chisholm M F, Nicolosi V, Pennycook T J, Corbin G J, Dellby N, Murfitt M F, Own C S, Szilagyi Z S, Oxley M P, Pantelides S T and Pennycook S J 2010 *Nature* **464** 571
[33] Zhao X, Kotakoski J, Meyer J C, Sutter E, Sutter P, Krasheninnikov A V, Kaiser U and Zhou W 2017 *MRS Bull.* **42** 667
[34] Dyck O, Kim S, Kalinin S V and Jesse S 2017 *Appl. Phys. Lett.* **111** 113104
[35] Zhao X, Dan J, Chen J, Ding Z, Zhou W, Loh K P and Pennycook S J 2018 *Adv. Mater.* **30** 1707281

[36] Yue R, Nie Y, Walsh L A, Addou R, Liang C, Lu N, Barton A T, Zhu H, Che Z, Barrera D, Cheng L, Cha P R, Chabal Y J, Hsu J W P, Kim J, Kim M J, Colombo L, Wallace R M, Cho K and Hinkle C L 2017 *2D Mater.* **4** 45019
[37] Eichfeld S M, Hossain L, Lin Y C, Piasecki A F, Kupp B, Birdwell A G, Burke R A, Lu N, Peng X, Li J, Azcatl A, McDonnell S, Wallace R M, Kim M J, Mayer T S, Redwing J M and Robinson J A 2015 *ACS Nano* **9** 2080
[38] Liu H J, Jiao L, Xie L, Yang F, Chen J L, Ho W K, Gao C L, Jia J F, Cui X D and Xie M H 2015 *2D Mater.* **2** 34004
[39] Egerton R F 2019 *Micron* **119** 72
[40] Lin J, Cretu O, Zhou W, Suenaga K, Prasai D, Bolotin K I, Cuong N T, Otani M, Okada S, Lupini A R, Idrobo J C, Caudel D, Burger A, Ghimire N J, Yan J, Mandrus D G, Pennycook S J and Pantelides S T 2014 *Nat. Nanotechnol.* **9** 436
[41] McKinley Jr, William A and Feshbach H 1948 *Phys. Rev.* **12** 1759
[42] Susi T, Kotakoski J, Kepaptsoglou D, Mangler C, Lovejoy T C, Krivanek O L, Zan R, Bangert U, Ayala P, Meyer J C and Ramasse Q 2014 *Phys. Rev. Lett.* **113** 115501
[43] Yoshimura A, Lamparski M, Kharche N and Meunier V 2018 *Nanoscale* **10** 2388
[44] Hong J, Pan Y, Hu Z, Lv D, Jin C, Ji W, Yuan J and Zhang Z 2017 *Nano Lett.* **17** 3383
[45] Meyer J C, Kisielowski C, Erni R, Rossell M D, Crommie M F and Zettl A 2008 *Nano Lett.* **8** 3582
[46] Nie Y, Liang C, Zhang K, Zhao R, Eichfeld S M, Cha P R, Colombo L, Robinson J A, Wallace R M and Cho K 2016 *2D Mater.* **3** 25029
[47] Nellist P D and Pennycook S J 2000 *Advances in Imaging and Electron Physics* vol. 113, edn. P W Hawkes (Elsevier) pp. 147–203
[48] Li S, Wang Y P, Ning S, Xu K, Pantelides S T, Zhou W and Lin J 2023 *Nano Lett.* **23** 1298